

Nonlinear Raman-Nath diffraction of inclined femtosecond laser by periodically poled lithium niobate nonlinear grating

Jiacheng Li(李嘉诚), Lihong Hong(洪丽红), Yu Zou(邹娱), Jianluo Chen(陈健洛), and Zhi-Yuan Li(李志远)
Citation: Chin. Phys. B, 2025, 34 (**5**): 054205. DOI: 10.1088/1674-1056/adb67f
http://cpb.iphy.ac.cn; http://iopscience.iop.org/cpb

What follows is a list of articles you may be interested in

A global model of intensity autocorrelation to determine laser pulse duration

Yufei Peng(彭雨菲), Liqiang Liu(刘励强), Lihong Hong(洪丽红), and Zhiyuan Li(李志远)
Chin. Phys. B, 2024, 33 (**5**): 054207. DOI: 10.1088/1674-1056/ad1c57

Simultaneous detection of CH_4 and CO_2 through dual modulation off-axis integrated cavity output spectroscopy

Yi-Xuan Liu(刘艺璇), Zhou-Bing Wang(王周兵), Xin-Xin Wei(韦欣欣), Jing-Jing Wang(王静静), Xin Meng(孟鑫), and Gui-Lin Mao(毛桂林)
Chin. Phys. B, 2023, 32 (**10**): 104209. DOI: 10.1088/1674-1056/acdac1

Phase-matched second-harmonic generation in hybrid polymer-LN waveguides

Zijie Wang(王梓杰), Bodong Liu(刘伯东), Chunhua Wang(王春华), and Huakang Yu(虞华康)
Chin. Phys. B, 2022, 31 (**10**): 104208. DOI: 10.1088/1674-1056/ac6edc

Second harmonic generation from precise diamond blade diced ridge waveguides

Hui Xu(徐慧), Ziqi Li(李子琦), Chi Pang(逄驰), Rang Li(李让), Genglin Li(李庚霖), Sh. Akhmadaliev, Shengqiang Zhou(周生强), Qingming Lu(路庆明), Yuechen Jia(贾曰辰), and Feng Chen(陈峰)
Chin. Phys. B, 2022, 31 (**9**): 094209. DOI: 10.1088/1674-1056/ac5242

A 45-μJ, 10-kHz, burst-mode picosecond optical parametric oscillator synchronously pumped at a second harmonic cavity

Chao Ma(马超), Ke Liu(刘可), Yong Bo(薄勇), Zhi-Min Wang(王志敏), Da-Fu Cui(崔大复), and Qin-Jun Peng(彭钦军)
Chin. Phys. B, 2022, 31 (**8**): 084206. DOI: 10.1088/1674-1056/ac6016

Nonlinear Raman–Nath diffraction of inclined femtosecond laser by periodically poled lithium niobate nonlinear grating

Jiacheng Li(李嘉诚)[1,†], Lihong Hong(洪丽红)[2,1,†,‡], Yu Zou(邹娱)[1], Jianluo Chen(陈健洛)[1], and Zhi-Yuan Li(李志远)[1]

[1] *School of Physics and Optoelectronics, South China University of Technology, Guangzhou* 510641, *China*
[2] *State Key Laboratory of Ultra-intense Laser Science and Technology, Shanghai Institute of Optics and Fine Mechanics, Chinese Academy of Sciences, Shanghai* 201800, *China*

(Received 10 December 2024; revised manuscript received 31 January 2025; accepted manuscript online 15 February 2025)

When a pump laser beam strikes the surface of a nonlinear crystal with modulated second-order nonlinearity, various nonlinear diffraction phenomena occur, with nonlinear Raman–Nath diffraction (NRND) being a prominent example. In this study, we use an 800-nm Ti:sapphire femtosecond laser beam to pump the surface of a periodically poled lithium niobate (PPLN) crystal thin-plate nonlinear grating. By rotating the crystal, we change the incidence angle and observe and measure the exit angle, polarization, and power of NRND spots on the other side of the crystal. The experiment shows that NRND characteristics are highly sensitive to the incidence angle of the pump laser beam, which are consistent with the theoretical prediction. We expect that this research will advance the understanding of nonlinear diffraction and provide valuable insights for nonlinear optical interaction in complicated geometric and physical configurations.

Keywords: nonlinear diffraction, second harmonic, quasi-phase matching, oblique incidence

PACS: 42.65.–k, 42.70.Mp, 52.35.Mw, 11.10.Lm

DOI: 10.1088/1674-1056/adb67f **CSTR:** 32038.14.CPB.adb67f

1. Introduction

In recent years, research on nonlinear Raman–Nath diffraction (NRND) has been emerging continuously. Recently a Maxwell-equation-based NRND model has been established, providing solid theoretical and experimental guidance to deeply understand the physics of NRND.[1] NRND is basically a noncollinear second-harmonic generation (SHG) process occurring when a fundamental-wave (FW) pump laser beam is shining upon a nonlinear grating made from microstructured nonlinear crystal such as periodically poled lithium niobate (PPLN). SHG signal originated from each LN domain with a size and pitch far larger the pump laser wavelength will be diffracted into various orientations and form a series of SHG beam spots with different orders.

Previous studies have shown that the influencing factors of NRND can be roughly classified into three categories: the optical properties of FW pump laser, the material properties of nonlinear crystal, and the geometric structure of nonlinear grating structure. In terms of the optical properties of FW pump laser beam, numerous studies have shown that factors such as beamwidth, wavelength, phase modulation, and the use of femtosecond laser sources can significantly influence NRND. Research has found that an increase in the beamwidth of FW pump beam significantly reduces the intensity of NRND,[2] while the wavelength of FW pump beam does not affect the diffraction angle of NRND but does impact the diffraction intensity.[2–4] Besides, it is found that pumping nonlinear crystals with femtosecond laser sources leads to a narrowing of SHG spectrum.[5,6] Moreover, the femtosecond laser sources can excite PPLN to produce a phenomenon of ultra-broadband NRND.[7] It is also found that the phase modulation of FW pump beam can be inherited by the phase of SHG.[8,9] All these studies indicate the significant impact of the characteristics of the FW pump laser on NRND.

On the other hand, theoretical research on nonlinear diffraction, especially regarding the diffraction angles, has been carried out extensively. However, there is still a need for in-depth study on the control effect of FW pump beam under the inclined incidence on NRND. Regarding the modulation of NRND by FW pump beam, the above studies[2–9] did not address the angle of incidence and polarization of FW pump beam, nor did the measurements of NRND phenomenon address the polarization angle of each order. In terms of the influence of nonlinear crystal structures on NRND, numerous studies have shown that factors such as the modulation type of nonlinear crystal,[10–12] domain structure,[13–15] doping,[16] and crystal type[17] all have a certain impact on NRND. What's more, a study using femtosecond lasers to pump PPLN forward and backward came into view, revealing the non-reciprocity of linear and nonlinear effects.[18] Finally, both experimental and theoretical studies on the effect

[†] These authors contributed equally to this work.
[‡] Corresponding author. E-mail: honglihong@siom.ac.cn

© 2025 Chinese Physical Society and IOP Publishing Ltd. All rights, including for text and data mining, AI training, and similar technologies, are reserved.

of duty cycle in nonlinear crystals with periodic polarization on NRND are reported.[2]

In this article, we will experimentally and theoretically investigate NRND from a PPLN thin-plate nonlinear grating pumped by 800-nm Ti:sapphire femtosecond laser beam at different inclined incidence angles. A simple theoretical model has been built to help interpret the experimental data for NRND. We focus on what happens to the NRND spot at different incidence angles, in particular, the power values and polarization angles of the diffractive spot in each order. This article aims to establish a closer relationship between FW pump beam and SHG diffraction beam and offer a promising route toward tunable SHG.[19]

2. Model and theory

In our theoretical model, which is in faithful consistence with the experiment configuration, we use a z-cut PPLN thin-plate crystal as the nonlinear medium, with the optical axis oriented in the z-direction. The crystal has a periodic polarization modulation that directly results in a positive and negative change of nonlinear polarizability tensor $\chi^{(2)}$ along the x-direction. The FW pump laser beam impinges on PPLN surface at a certain angle of incidence in the XOZ plane, as shown in Fig. 1. The second-order nonlinearity modulation is along the x axis direction, and the positive and negative LN domains are homogeneous along the y axis direction. Through the modulation of the Glan prism, as illustrated in Fig. 2, the femtosecond laser beam incident on the surface of PPLN thin-plate is horizontally polarized, and the angle of incidence is α. The FW laser beam refracted and transporting inside PPLN interacts with LN domains, ignites SHG process, and produces SHG beam with wave vector k_2, which then exits through the rear surface of PPLN thin-plate, with the exit angle being γ_m.

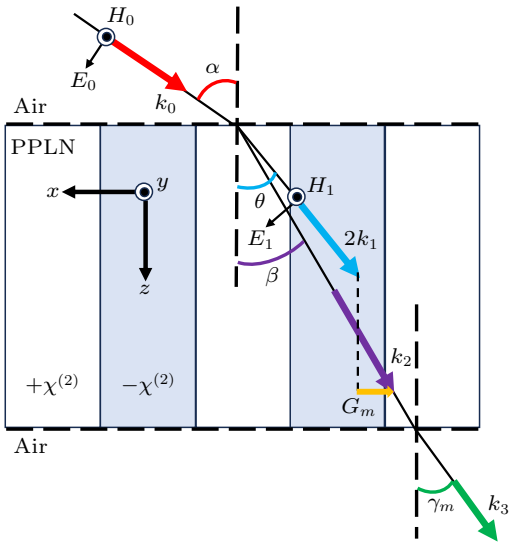


Fig. 1. The cross-sectional view of the light propagation and electromagnetic field analysis of incident wave, transmission wave and SHG from air to PPLN crystal, and from crystal to air, and the phase matching diagram associated reciprocal lattice vector in the cases of pump laser beam oblique incidence.

The equation governing the electromagnetic field temporal-spatial evolution of FW pump beam and SHG beams in the current nonmagnetic, free-charge-free homogeneous medium can be derived from Maxwell's system of equations:

$$\nabla^2 \boldsymbol{E}(\boldsymbol{r},t) = \mu_0 \varepsilon_0 \frac{\partial^2 \boldsymbol{E}(\boldsymbol{r},t)}{\partial t^2} + \mu_0 \frac{\partial \boldsymbol{P}(\boldsymbol{r},t)}{\partial t^2}, \tag{1}$$

we express the electric field intensity vectors and polarization intensity vectors as summation formulas upon the linear and nonlinear components:

$$\boldsymbol{E}(\boldsymbol{r},t) = \sum\nolimits_n \boldsymbol{E}(\omega_n,\boldsymbol{r})\, \mathrm{e}^{-\mathrm{i}\omega_n t}, \tag{2}$$

$$\boldsymbol{P}(\boldsymbol{r},t) = \sum\nolimits_n \boldsymbol{P}(\omega_n,\boldsymbol{r})\, \mathrm{e}^{-\mathrm{i}\omega_n t}, \tag{3}$$

$$\boldsymbol{P}(\omega_n,\boldsymbol{r}) = \boldsymbol{P}_{\mathrm{L}}(\omega_2,\boldsymbol{r}) + \boldsymbol{P}_{\mathrm{NL}}(\omega_2,\boldsymbol{r}), \tag{4}$$

$$\boldsymbol{P}_{\mathrm{NL}}(\omega_2,\boldsymbol{r}) = \varepsilon_0 \chi^{(2)}(x) : \boldsymbol{E}_{10}\boldsymbol{E}_{10}, \tag{5}$$

where $\boldsymbol{P}_{\mathrm{L}}(\omega_2,\boldsymbol{r})$ is the linear polarization intensity vector, $\boldsymbol{P}_{\mathrm{NL}}(\omega_2,\boldsymbol{r})$ is the nonlinear polarization intensity vector, $\chi^{(2)}(x)$ is the second-order nonlinear susceptibility tensor, and $\boldsymbol{E}_{10}$ is FW pump beam electric field vector.

Similarly, we express the second-order nonlinear polarization tensor of PPLN as summation formula upon the reciprocal lattice vectors G_m:

$$\chi^{(2)}(x) = \sum\nolimits_m \chi^{(2)}(G_m)\, \mathrm{e}^{\mathrm{i}G_m x}, \tag{6}$$

substituting Eqs. (2)–(5) into Eq. (1), we can derive different equations satisfied by the SHG beam electric field and its explicit scalar expression obtained through integration

$$\frac{\partial \boldsymbol{E}_{20}(\omega_2,G_m,z)}{\partial z} = \frac{\mathrm{i}\omega_2^2}{k_{2z,m}c^2}\left[d(G_m) : \boldsymbol{E}_{10}\boldsymbol{E}_{10}\right] \mathrm{e}^{\mathrm{i}\Delta k_{z,m} z}, \tag{7}$$

$$E_{20}(\omega_2,G_m,z) = \frac{\omega_2^2}{\Delta k_{z,m} k_{2z,m} c^2} d_{\mathrm{eff}}(G_m) \left| E_{10} \right|^2 \left(\mathrm{e}^{\mathrm{i}\Delta k_{z,m} z} - 1 \right), \tag{8}$$

where $\boldsymbol{E}_{20}(\omega_2,G_m,z)$ represents SHG beam electric field inside the crystal and $d(G_m)$ is second-order nonlinear coefficient tensor of LN crystal. $d_{\mathrm{eff}}(G_m)$ represents the effective second-order nonlinear coefficient which equals half of $\chi^{(2)}(G_m)$ for the specific reciprocal lattice vector. $G_m = 2\pi m/\Lambda$ for PPLN, and m is the diffraction order, Λ is the polarization period of PPLN. The power of NRND can be obtained simply by taking the square modulus of Eq. (8). From the above equation, we can see that, with the wavelength and power of FW pump beam fixed, the power of NRND is determined by the diffraction order and the effective nonlinear coefficient $d_{\mathrm{eff}}(G_m)$. Due to the relatively small variation of the effective nonlinear coefficient $d_{\mathrm{eff}}(G_m)$, the primary influencing factor is still the diffraction order. Clearly, as the diffraction order increases, the magnitude of the SHG wave vector will increase, constrained by the transverse phase matching

conditions of NRND, leading to a decrease in the diffraction intensity of NRND.

According to the transverse phase matching condition for NRND:

$$2k_{1x} + G_m = k_{2x}, \tag{9}$$

we can solve the expression for the angle γ_m at which the diffracted light deviates from the 0th order for NRND using Eq. (9) and Fresnel formula

$$\gamma_m = \arcsin\left(\sin\alpha + \frac{G_m}{4\pi}\lambda\right). \tag{10}$$

We find that the magnitude of γ_m is related to the incidence angle α and diffraction order m, so we define two offset amounts. One is the angular offset amount ($\Delta\gamma_1$) under different incidence angles with the same diffraction order, and the other is the angular offset amount ($\Delta\gamma_2$) of the positive and negative diffraction orders with the same incidence angle. The two quantities are derived as

$$\Delta\gamma_1^{\alpha} = \arcsin\left(\sin\alpha + \frac{G_m}{4\pi}\lambda\right) - \arcsin\left(\frac{G_m}{4\pi}\lambda\right), \tag{11}$$

$$\Delta\gamma_2^{m} = \arcsin\left(\sin\alpha + \frac{G_m}{4\pi}\lambda\right) - \arcsin\left(\sin\alpha + \frac{G_{-m}}{4\pi}\lambda\right), \tag{12}$$

where $\Delta\gamma_1^{\alpha}$ represents the angular offset of each order diffraction angles between the case where the incidence angle is not 0° and the case where the incidence angle is 0°. $\Delta\gamma_2^{m}$ is the angular offset of each incidence angle between negative orders and positive orders.

From the above equations, we can clearly see that when the order is 0, the diffraction angle of NRND equals the incidence angle, in other words, the 0th order NRND is collinear with the incident light. When the order is not 0, the diffraction angle of NRND is directly related with both the incidence angle and the order.

We take the ordinary light vector and the extraordinary light vector and perform a vector dot operation with the electric field strength vector we have obtained, and then calculate the polarization components of NRND within the crystal:

$$\frac{\partial E_{20}^{\mathrm{o/e}}(\omega_2, G_m, z)}{\partial z} = \left|\boldsymbol{a}^{\mathrm{o/e}}(\omega_2, G_m)\cdot\frac{\partial \boldsymbol{E}_{20}(\omega_2, G_m, z)}{\partial z}\right|. \tag{13}$$

Due to the difference in the transmittance coefficient of ordinary light (o-light) and extraordinary light (e-light) in the stage of incidence and exiting, the polarization angle will be changed at both incident and exit stages. Based on the different transmittance through PPLN crystal for the electric field strengths of different polarization directions, we calculate the polarization angle δ of NRND outside the crystal:

$$\delta = \arctan\left(\frac{\left|t_{\mathrm{o}}E_{20}^{\mathrm{o}}(\omega_2, G_m, z)\right|}{\left|t_{\mathrm{e}}E_{20}^{\mathrm{e}}(\omega_2, G_m, z)\right|}\right), \tag{14}$$

where t_{o} is the transmittance of ordinary light field amplitude at the interface between PPLN and air, and t_{e} is the transmittance of extraordinary light field amplitude.

Until this stage, we have built a theoretical method allowing analysis and solution of the diffraction angle, power, and polarization angle of NRND against a PPLN thin-plate nonlinear crystal, and this method would help to provide a foundation for our subsequent experimental design.

3. Experiment and discussions

Our experiment setup is shown in Fig. 2. In our experiment, the nonlinear crystal we use is a z-cut PPLN thin-plate crystal with Λ of 6.97 μm, and its dimensions are 20 mm (x) × 5 mm (y) × 1 mm (z). The PPLN sample can be prepared via the standard electric poling technique.[1,2,20–22] The optical axis of the crystal is oriented in the z-axis direction, and the modulation direction is in the x-axis direction. We use a Ti:sapphire femtosecond laser to serve as the pump light, with a central wavelength of 800 nm, a pulse duration of 50 fs, a spectral width of 24 nm (in 3 dB), and an average power of 3 W in maximum. To prevent excessive power from damaging the device, we use a half-wave plate to attenuate the pump light, ensuring that the power incident on the crystal surface is maintained at 0.82 W. Before the lens, a Glan prism is placed to fix the polarization state of the pump light to horizontal polarization[23,24] (i.e., parallel to the x-axis direction of PPLN nonlinear grating), eliminating the influence of polarization on the experiment. The PPLN sample together with its holder is placed on a rotating stage that allows one to rotate PPLN to precisely change the angle of oblique incidence with the XOZ plane while maintaining the incident light to be perpendicular to the LN domain extension direction (y-axis). Behind the crystal, we place a long-pass filter that only transmits wavelengths above 500 nm to filter out stray light and transmitted light at 800 nm. Finally, the NRND SHG beam from the crystal is projected onto an observation screen located 38 cm away, and the pattern is recorded using a camera.

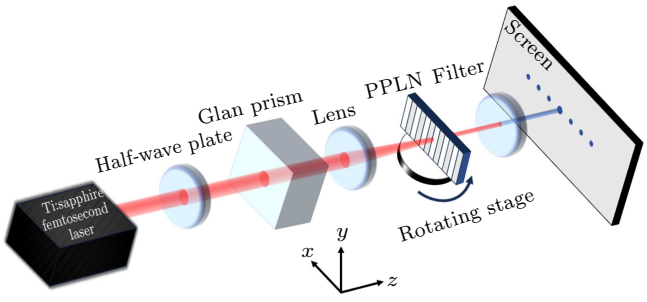


Fig. 2. Experiment setup to study NRND of PPLN nonlinear grating illuminated by an obliquely incident 800-nm Ti:sapphire femtosecond laser beam.

We have observed a series of blue spots occurring in the screen, as displayed in Fig. 3(a). They are recognized to be

the NRND SHG beam spots. We measure the diffraction angles for different orders of NRND as a function of the incidence angles of pump beam, and the results are in Fig. 3(b). Obviously, as the incidence angle increases, the spot of each order spreads out to both positive and negative sides which is in great agreement with theoretical prediction and physical diagram of phenomenon. We can see that the angular position of NRND spot of the 0th order remains strictly equal to the incidence angle when the incidence angle changes. At the incidence angle of 0°, the diffraction spots of positive and negative order NRND show a symmetric pattern. The diffraction angles of ±1st, ±2nd, ±3rd, ±4th, and ±5th orders are 3.3°, 6.6°, 10.0°, 13.6°, and 16.7°, respectively, which are in excellent agreement with our theoretical predictions of 3.3°, 6.6°, and 9.9°, 13.3°, and 16.7°.

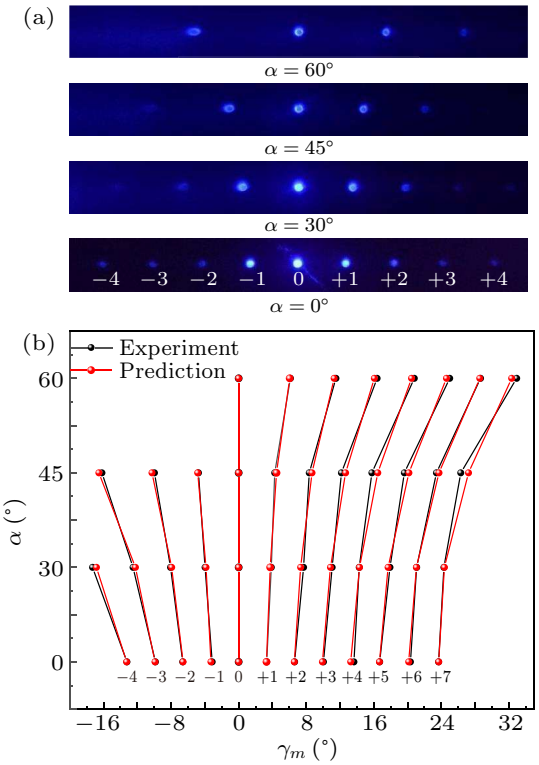


Fig. 3. (a) Experiment images showing the observed NRND SHG spots as a function of the incidence angle. From bottom to top, the phenomenon is plotted for angles of incidence 0°, 30°, 45°, and 60° in order. (b) Comparison of theoretical predicted angle and experimentally measured angle of NRND at different incidence angles and for various diffraction orders.

From the experimental phenomenon, it can be seen that with the increase of the incidence angle, the diffraction angle for positive and negative NRND orders becomes different, and this asymmetry can be described by the quantity $\Delta\gamma_1^{\alpha}$. Moreover, $\Delta\gamma_1^{\alpha}$ gradually expands for each order of NRND with respect to the increased value of oblique angle. For the +1st order, the differences $\Delta\gamma_1^{\alpha}$ between the diffraction angles of NRND at incidence angles of 30°, 45°, and 60° and the diffraction angle at incidence angles of 0° are 0.6°, 1.0°, and 2.8° respectively. These values show good numerical proximity and consistent trends with the theoretical values of 0.4°, 1.2°, and 2.7°. Similarly, for the +2nd order, $\Delta\gamma_1^{\alpha}$ between the diffraction angles of NRND at incidence angles of 30°, 45°, and 60° and the diffraction angle at incidence angles of 0° are 1.1°, 1.7°, and 4.9° respectively, which is consistent with the theoretical values of 0.8°, 2.1°, and 4.7°. For the +3rd, +4th, +5th orders, and higher orders, as well as the negative orders, the diffraction spots of NRND at the same order all exhibit a widening effect on both sides. At the same time, when the angle of incidence is the same, $\Delta\gamma_1^{\alpha}$ also shows a gradual increasing trend with the increase of the order. At the incidence angel of 30°, $\Delta\gamma_1^{\alpha}$ for the −1st, −2nd, −3rd, and −4th orders are 0.8°, 1.4°, 2.6°, and 4.1°. At the incidence angel of 45°, $\Delta\gamma_1^{\alpha}$ for the −1st, −2nd, and −3rd orders are 1.6°, 3.4°, and 6.3°. It can be seen that the amount of $\Delta\gamma_1^{\alpha}$ increases with the increase in the incidence angle for each order and with the increase in the order for each incidence angle, and there is a good agreement with the theoretical predictions in terms of both the numerical values of the angular differences and the trend of change.

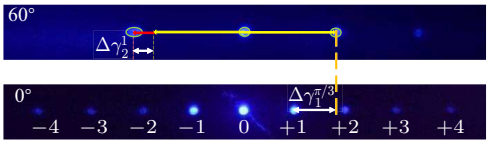


Fig. 4. Angular offset between the incidence angle of 0° and 60°. $\Delta\gamma_1^{\pi/3}$ represents the difference between the +1st order diffraction angle at 60° incidence and the +1st order diffraction angle at 0° incidence, $\Delta\gamma_1^{\alpha}$ represents the angular offset in any same order between the incidence angle of α and 0°. The yellow line represents the magnitude of the +1st order diffraction angle at 60° incidence, where $\Delta\gamma_2^1$ and $\Delta\gamma_2^m$ represent the angular offset in the ±1st and ±m-th order at any same incidence angle.

On the other hand, it can be found from Fig. 3(a) that the diffraction angle of the negative order is larger than that of the positive order, and this asymmetry can be described by the quantity $\Delta\gamma_2^m$. The phenomenon is most obvious when the incidence angle is 60°, as illustrated in Fig. 4. At the incidence angle of 30°, NRND is slightly offset to negative order side with $\Delta\gamma_2^m$ of 0.1°, 0.4°, 1.4°, and 3.0° for orders ±1st, ±2nd, ±3rd, and ±4th, respectively, which show consistent patterns with our theoretical predictions of 0.1°, 0.6°, 1.4°, and 2.5°, all of which exhibit that the higher the order, the larger the offset angle. At the incidence angle of 45°, $\Delta\gamma_2^m$ of orders ±1st, ±2nd, and ±3rd is 0.5°, 1.6°, and 4.0°, respectively, which show the same increasing pattern as our theoretical predictions of 0.4°, 1.6°, and 3.9°. Finally, $\Delta\gamma_1^{\alpha}$ of +1st to +7th order NRND at the incidence angle of 60° are 0.1°, 0.2°, 0.3°, 0.3°, 0.4°, 0.1°, 0.6°, respectively, with offset angle values of more than 0.6°. In conclusion, compared to 0° incidence, the NRND spots of each diffraction order exhibit varying degrees of offset when the incidence angle is not 0°, and the degree of offset increases as the incidence angle increases.

We have measured all the powers of NRND using a sensitive power meter that can detect a weak power down to the nW level. Besides, we have performed numerical calculation

on these quantities. The comparison results of theory and experiment are shown in Fig. 5.

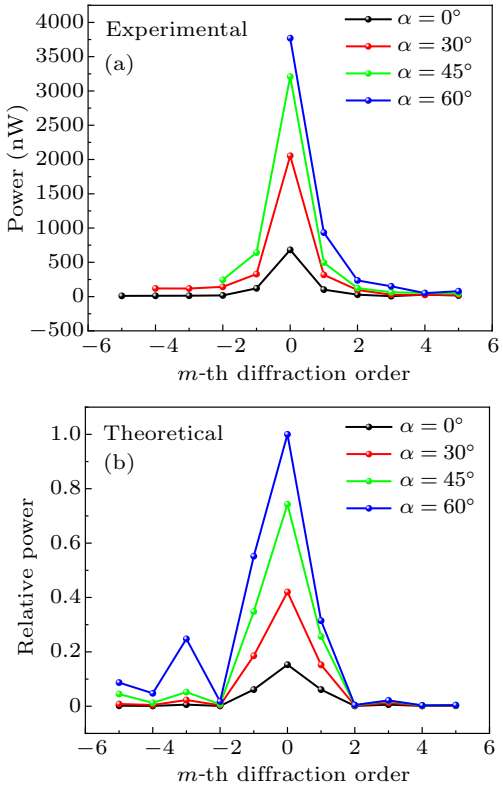


Fig. 5. (a) Experimentally measured power of NRND SHG beam output signals corresponding to different diffraction orders at four incidence angles. (b) Theoretically predicted relative power of NRND SHG output signals corresponding to different diffraction orders at four incidence angles.

We notice that in the experiment, nonlinear Cherenkov radiation is generated and observed simultaneously together with NRND. Under large incidence angles, the nonlinear Cherenkov radiation pattern experiences significant lateral shifts,[25,26] which in turn will mix the diffraction pattern of NRND and thus affect the quantitative observation and evaluation of NRND. As a result, when the incidence angle is 60°, it is difficult to observe negative order NRND phenomena because the background blue signal from nonlinear Cherenkov radiation is too large.

From Fig. 5, we find several interesting phenomena. First, no matter what is the incidence angle for oblique incidence, the diffraction power of NRND basically decreases with the increase of the order. When NRND order is 0, the power value of the diffraction spot is the largest. Second, the diffraction power at 0°, 30°, 45°, 60° is 682 nW, 2054 nW, 3210 nW, and 3770 nW respectively for the 0th order, which increases with the growth of the incidence angle. Similarly, this behavior is also reflected in other orders. The diffraction power at the four incidence angles is 101.2 nW, 317.6 nW, 495.0 nW, and 934.0 nW respectively for the +1st order, 27.3 nW, 95.8 nW, 123.4 nW, and 236.1 nW respectively for the +2nd order, and 5.8 nW, 28.2 nW, 63.4 nW, and 150.2 nW respectively for the +3rd order, 28.09 nW, 24.7 nW, 53.3 nW, and 50.8 nW, respectively for the +4th order, and 16.3 nW, 24.8 nW, 44.0 nW, and 78.7 nW respectively for the +5th order. This variation phenomenon can be described by $d_{\text{eff}}(G_m)$ in Eq. (8), which increases with the increase of the incidence angle, then the power of SHG which is proportional to the square of the mold of $E_{20}(\omega_2, G_m, z)$ and $d_{\text{eff}}(G_m)$, showing a upward trend with the increase of the incidence angle.

Third, the theoretical result in Fig. 5(b) shows that the power of the odd order is higher than the power of the even order around it, and the phenomenon of negative orders is more obvious than that of positive orders. The power of the 0th order is greater than that of the +1st and −1st orders, the power of the −3rd order is greater than that of the −2nd and −4th orders, and the power of the +3rd order is greater than that of the +2nd and +4th orders. Most obviously, when the incidence angle is 60°, the power of the −3rd order is much higher than that of the −2nd and −4th orders. We can also find it in our experiment. When the incidence angle is 30°, the power of the +5th order is 24.82 nW and it is a little bigger than 24.74 nW for the power of the +4th order. What is more, at the incidence angle of 60°, the power of the +5th order and +4th order is 78.7 nW and 50.8 nW respectively. At the incidence angle of 30°, the power of the negative orders including −2nd, −3rd, −4th are 142.5 nW, 117.8 nW, 118.8 nW, which is much stronger than the positive orders, with the power of the +2nd, +3rd, and +4th orders are 95.8 nW, 28.23 nW and 24.74 nW.

We observed that the NRND spot reaches a peak power of 3770 nW, at an incidence angle of 60° and diffraction order of 0th. The incident beam power on the PPLN surface remains at 0.82 W, controlled by a half-wave plate positioned after the Ti:sapphire femtosecond laser. This indicates that the maximum efficiency of NRND can approach 4.6×10^{-6}. As the incidence angle increases, the overall efficiency gradually increases from 1.26×10^{-6} to 7.0×10^{-6}, which is consistent with our predictions. Although this number is still not a high value compared to usual collinear QPM-SHG processes ($\sim$ 30%), it has already relatively objective conversion efficiency value for partial phase matching process.

We use a bias detector to detect the polarization state of each order of NRND diffraction spots. We find that each order is linearly polarized, and the polarization angle is displayed in Fig. 6. The polarization angle of diffraction spots in each order basically decreases with the increase of incidence angle. At the 0th order, the polarization angle of NRND changes with the angle of incidence in the order of 52.2°, 34.9°, 27.5°, and 25.0° respectively, which shows a decrease with the increase of the incidence angle. The polarization angles are 19.0°, 19.2°, 14.3°, and 12.0°, respectively for the +1st order, 49.6°, 37.9°, 45.1°, and 36.0° respectively for the +2nd order, 57.9°, 52.2°, 48.9°, and 25.3° respectively for the +3rd order, 48.8°, 42.0°, 39.7°, and 41.4°, respectively for the +4th order, 44.9°, 40.3°, 41.5°, and 43.0°, respectively for the ±5th order. From this, we can see that the experimental curves have

a downward trend. And the polarization angles of each order are relatively close, especially in the 0th, 2nd, 3rd, 4th and 5th orders with each incidence angle, which can be described by the $d(G_m) : \boldsymbol{E}_{10}\boldsymbol{E}_{10}$ in Eq. (7). In more details, the $d(G_m) : \boldsymbol{E}_{10}\boldsymbol{E}_{10}$ is a dyadic tensor which can determine the electric field vector direction of SHG beam. When the incidence angle increases, this parameter has a greater component of the e-light direction than o-light, then the polarization angle decreases in Eq. (14).

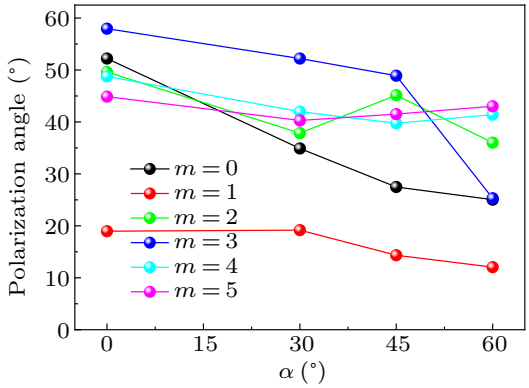


Fig. 6. Experimentally measured polarization angle of NRND SHG beam output signals with diffraction orders corresponding to different incidence angles.

4. Conclusions

In summary, we have used an 800-nm Ti:sapphire femtosecond laser beam to obliquely pump a PPLN crystal nonlinear grating with a polarization period of 6.97 μm, and investigated the variation and sensitivity of NRND to the oblique angle of incidence. Starting from Maxwell's equations, we derive the expression for the electric field intensity of each NRND diffraction order and obtained an analytical expression for the diffraction angle and polarization angle under the transverse phase matching conditions involves in the NRND process. In our experiments, we have successfully observed clear NRND patterns as characterized by the diffraction angles, power, and polarization information of different diffraction orders at different oblique incidence angles. The experiment results show good agreement with theoretical predictions in terms of the diffraction angles and power. In particular, the diffraction angle shows an obvious asymmetry for positive and negative orders, and this asymmetry is the most pronounced at large oblique incidence angle. The diffraction power of various NRND spots shows a fluctuation-decaying behavior when the diffraction order increases from the 0th order to higher orders. In short, the experiment shows that the NRND characteristics are highly sensitive to the incidence angle of the pump laser beam, which are consistent with the theoretical prediction. We expect that this research of NRND from a PPLN nonlinear grating as excited by a high-peak power femtosecond laser beam under the oblique incidence pump configuration will advance the understanding of nonlinear diffraction and provide valuable insights for nonlinear optical interaction in complicated geometric and physical configurations.

Acknowledgements

Project supported by the Science and Technology Project of Guangdong Province, China (Grant No. 2020B010190001), the National Natural Science Foundation of China (Grant No. 12434016), and the National Funded Postdoctoral Researcher Program (Grant No. GZB20240785).

References

[1] Hong L H, Zou Y, Li J C, Chen J L and Li Z Y 2024 *J. Opt. Soc. Am. B* **41** 2562
[2] Sheng Y, Kong Q, Wang W J, Kalinowski K and Krolikowski W 2012 *J. Phys. B: At. Mol. Opt. Phys.* **45** 055401
[3] Chen Y P, Dang W R, Zheng Y L, Chen X F and Deng X W 2013 *Opt. Lett.* **38** 2298
[4] Chen Y S, Liu Y X, Zhao R W, Xu T X, Sheng Y and Xu T F 2022 *Crystal Research and Technology* **57** 2100193
[5] Vyunishev A M, Slabko V V, Baturin I S, Akhmatkhanov A R and Shur V Y 2014 *Opt. Lett.* **39** 4231
[6] Vyunishev A M, Arkhipkin V G, Slabko V V, Baturin I S, Akhmatkhanov A R, Shur V Y and Chirkin A S 2015 *Opt. Lett.* **40** 4002
[7] Hong L H, Chen B Q, Hu C Y and Li Z Y 2022 *Photonics Research* **10** 905
[8] Liu H G, Li J, Zhao X H, Zheng Y L, and Chen X F 2017 *Conference on Lasers and Electro-Optics (CLEO)*, May 14–19, 2017, San Jose, CA, USA, p. 1
[9] Zhou H Q, Liu H G, Sang M H, Li J and Chen X F 2017 *Opt. Express* **25** 3774
[10] Wang W J, Sheng Y, Roppo V, Chen Z H, Niu X Y and Krolikowski W 2013 *Opt. Express* **21** 18671
[11] Vyunishev A M, Arkhipkin V G and Chirkin A S 2015 *J. Opt. Soc. Am. B* **32** 2411
[12] Karpinski P, Chen X, Shvedov V, Hnatovsky C, Grisard A, Lallier E, Davies B L, Krolikowski W and Sheng Y 2015 *Opt. Express* **23** 14903
[13] Chen C D, Feng C and Hu X P 2019 *J. Opt.* **21** 035501
[14] Sheng Y, Wang W J, Shiloh R, Roppo V, Arie A and Krolikowski W 2011 *Opt. Lett.* **36** 3266
[15] Kalinowski K, Roppo V, Lukasiewicz T, Swirkowicz M, Sheng Y and Krolikowski W 2012 *Appl. Phys. B* **109** 557
[16] Shui T, Yang W X and Li L 2019 *Opt. Express* **27** 24693
[17] Smirnov V A and Vostrikova L I 2016 13*th International Scientific-Technical Conference on Actual Problems of Electronics Instrument Engineering (APEIE)*, October 3–6, 2016, Novosibirsk, Russia, p. 379
[18] Hong L H, Zou Y, Ji Z T and Li Z Y 2024 *Phys. Rev. Lett.* **133** 223801
[19] Aleksandrovsky A S, Vyunishev A M, Slabko V V, Zaitsev A I and Zamkov A V 2009 *Opt. Commun.* **282** 2263
[20] Chen B Q, Ren M L, Liu R J, Zhang C, Sheng Y, Ma B Q and Li Z Y 2014 *Light Sci. Appl.* **3** e189
[21] Chen B Q, Zhang C, Hu C Y, Liu R J and Li Z Y 2015 *Phys. Rev. Lett.* **115** 083902
[22] Ren M L, Ma D L and Li Z Y 2011 *Opt. Lett.* **36** 3696
[23] Saltiel S M, Neshev D N, Krolikowski W, Arie A, and Kivshar Y S 2009 11*th International Conference on Transparent Optical Networks*, 28 June–2 July, 2009, Ponta Delgada, Portugal, p. 1
[24] Trull J, Cojocaru C, Fischer R, Saltiel S M, Staliunas K, Herrero R, Vilaseca R, Neshev D N, Krolikowski W and Kivshar Y S 2007 *Opt. Express* **15** 15868
[25] Wang W J, Sheng Y, Kong Y F, Arie A and Krolikowski W 2010 *Opt. Lett.* **35** 3790
[26] Hong L H, Chen B Q, Hu C Y, He P and Li Z Y 2022 *Phys. Rev. Appl.* **18** 044063